

Journal of Materials Chemistry C

Accepted Manuscript



This is an *Accepted Manuscript*, which has been through the Royal Society of Chemistry peer review process and has been accepted for publication.

Accepted Manuscripts are published online shortly after acceptance, before technical editing, formatting and proof reading. Using this free service, authors can make their results available to the community, in citable form, before we publish the edited article. We will replace this *Accepted Manuscript* with the edited and formatted *Advance Article* as soon as it is available.

You can find more information about *Accepted Manuscripts* in the [Information for Authors](#).

Please note that technical editing may introduce minor changes to the text and/or graphics, which may alter content. The journal's standard [Terms & Conditions](#) and the [Ethical guidelines](#) still apply. In no event shall the Royal Society of Chemistry be held responsible for any errors or omissions in this *Accepted Manuscript* or any consequences arising from the use of any information it contains.

ARTICLE

Cite this:
10.1039/x0xx00000x

DOI:

Eu(III)/Eu(II)-doped (Ca_{0.7}Sr_{0.3})CO₃ phosphors with vaterite/calcite/aragonite forms as shock/temperature detectors.

Received 00th January 2012,
Accepted 00th January 2012

V. Blanco-Gutierrez,[†] A. Demourgues,[†] V. Jubera,^{†,‡} M. Gaudon^{*,†,‡}

DOI: 10.1039/x0xx00000x

www.rsc.org/

Pure metastable Eu(III)-doped (Ca_{0.7}Sr_{0.3})CO₃ vaterite phase has been obtained by the precipitation method. After thermal treatment of this phase, the carbonate crystallizes with calcite structure. Moreover, with the incorporation of 30 mol % of Sr that tends to stabilize the aragonite structure, both vaterite and calcite phases are able to transform easily into this high-pressure form by mechanical treatment. Hence, for this single composition, the three allotropic forms are achieved and can be compared. Photoluminescence studies indicate the stabilization of the Eu ions in the carbonates obtained whatever the allotropic form, at the trivalent oxidation state. Significantly different luminescent properties have been found depending on the carbonate structure, which are associated with the various local environments of the doping element. This offers the possibility to employ these Eu(III)-doped samples as shock and/or temperature detector. In addition, the use of CaH₂ reducing agent allowed reducing at low temperature the main part of the Eu(III) content into Eu(II) in the three different carbonate forms. Photoluminescence studies were also performed in these Eu(II)-doped samples and show slightly different emission spectra for the three crystalline structures.

Introduction

Calcium carbonate (CaCO₃) is one of the most abundant compounds in the nature that is incorporated into everyday materials like fillers in plastics¹ and also offers some challenging applications such as CO₂ sequestration or nuclear waste disposal.^{2,3} It presents three anhydrous allotropic forms: vaterite (*P6₃/mmc* S. G.) which is the most kinetically favored, calcite (*R-3c* S. G.), which is the most stable at ambient conditions and aragonite (*Pmcn* S. G.) obtained at high-pressure values and metastable at ambient conditions with very slow kinetic of transformation into calcite phase.⁴ The transformation into the aragonite phase only occurs at very high pressure values⁵ with an increasing coordination number up to 9 for Ca²⁺ cation.⁶ However, it has been already reported⁵ the possibility to decrease this transformation pressure by doping the compound with Sr²⁺ to form (Ca,Sr)CO₃. In this case, the aragonite phase is stabilized⁷ due to the higher ionic radii and lower electronegativity of Sr²⁺ in comparison with Ca²⁺ cation. On the other hand, inorganic luminescent materials containing rare-earth elements are extensively investigated as they exhibit

high luminescent response and good chemical stability. Among all of luminescence activators, europium is one of the most employed as phosphor because of its luminescence in the visible range.⁸⁻¹⁰ Taking into account the proximity of the Eu³⁺ or Eu²⁺ ionic radii (0.95 Å and 1.17 Å respectively, in octahedral site) in comparison to that of Ca²⁺ or Sr²⁺ (1.00 and 1.16 Å respectively, in octahedral site),¹¹ no difficulties may be expected in its incorporation into a (Ca,Sr)CO₃ structure. In this sense, several studies report the possible Ca²⁺ cation substitution to form CaCO₃:Eu solid-solution,¹²⁻¹⁶ or SrCO₃ solid-solution,¹⁷⁻¹⁸ for the mentioned allotropic forms of the carbonate. Depending on the experimental synthesis, the europium element can be stabilized at the trivalent or divalent oxidation state whatever the host matrix. When Eu³⁺ ion is introduced in a matrix, the luminescence emission spectrum is characterized by groups of lines peaking at around 610 nm and the radiative process is due to 4f-4f transitions.⁸⁻¹⁰ In the case of Eu²⁺, the emission is characterized by a large and intense band centered in the blue green range and associated to the allowed 5d-4f radiative transitions.¹⁹

The co-precipitation method characterized by the employment of soft synthesis conditions,^{7,13} seems to be a suitable

alternative process to the solid-state route, to prepare calcium carbonate phases that exhibit a low chemical stability, i.e. they decomposes at moderate temperatures around 800 °C. Furthermore, materials prepared by the co-precipitation method present good crystallinity which is usually associated with good photoluminescence properties.^{20,21} In this kind of synthesis routes, the reactants homogeneity in atomic level is ensured by Fick diffusion in the starting solution. Hence, it is possible to obtain kinetically favored metastable phases which are sensitive to evolve to another one while temperature or pressure is applied.

It is presented in this work how Eu(III)-doped ($\text{Ca}_{0.7}\text{Sr}_{0.3}\text{CO}_3$) compound with vaterite, calcite or aragonite form can be obtained directly by co-precipitation and employing additional thermal or mechanical treatment in the case of calcite and aragonite phases. It is reported as well the possibility to reduce at low temperature part of the Eu(III) into Eu(II) in the three carbonate forms by using CaH_2 as reducing agent. Structural and optical characterizations (luminescent properties) are reported as function of the allotropic form of the synthesized carbonate and the oxidation degree of the phosphor doping. Since it is possible to transit from one to another allotropic form by employing heat or pressure, the thermochromic and piezochromic properties of the doped carbonates, are finally discussed.

Experimental

Synthesis process

Vaterite, calcite and aragonite ($\text{Ca,Sr}\text{CO}_3\text{:Eu}^{3+}$) samples were prepared and labeled as V1, C1 and A1, respectively. Our preliminary studies indicate the chosen Ca:Sr molar ratio of 70:30 allows stabilizing at room temperature the three crystalline forms. The europium-doped carbonate with Eu/(Ca+Sr) molar ratio equal to 1%, were directly obtained by the co-precipitation method. $\text{Ca}(\text{NO}_3)_2 \cdot 4\text{H}_2\text{O}$ and $\text{Sr}(\text{NO}_3)_2$ (Aldrich) were used as alkaline-earth precursors and Eu_2O_3 as the rare-earth source. An initial Eu^{3+} nitrate solution was made from the oxide and HNO_3 . Then, a 2M aqueous solution of Ca^{2+} , Sr^{2+} and Eu^{3+} was prepared using stoichiometric amounts of the corresponding metals. A 3M aqueous solution of NH_4HCO_3 in double molar excess was added drop by drop to the cationic solution leading to the precipitation of a white product that was matured under stirring at 0°C for 45 min to get the pure vaterite form (V1 sample). Different portions of V1 sample were thermally treated from 200 to 700°C for 1 h. The employed heating rate was 7°C/min and the final product was cooled down at room temperature. These experiments have shown that a thermal treatment of 400°C (1 h) can be employed to obtain the calcite phase from vaterite (sample C1). Afterwards, indifferently V1 or C1 sample can be mechanically treated by ball-milling in agate container for 90 min to obtain aragonite phase (A1 sample). The synthesis strategy to obtain the three allotropic forms of the Eu(III)-doped ($\text{Ca,Sr}\text{CO}_3$) compound can be followed by the scheme depicted in Figure 1a.

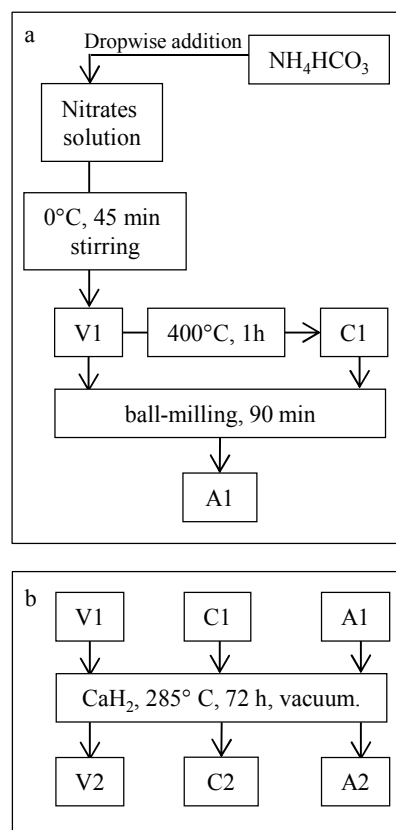


Figure 1. Experimental strategies to obtain V1, C1 and A1 samples (a) and V2, C2 and A2 samples (b).

An additional treatment was developed to force the reduction of the europium ions at the divalent oxidation state. Vaterite, calcite and aragonite samples containing Eu(II) were prepared and labeled as V2, C2 and A2, respectively. For such purpose, CaH_2 was employed as reducing agent. The stoichiometric redox reaction between the hydride and the Eu(III)-doped carbonate requires very low hydride volume in comparison with that of the carbonate, what hinders a total surface contact between both reactants. Therefore, in order to favor this surface contact, the reducing agent was added in a five times molar excess. For each sample, both carbonate and hydride compounds were ground in agate mortar to prepare a compact pellet that was placed in a quartz tube provided of an opening-key. All this manipulation was performed under Ar in a glove-box. Then, the tube was sealed in vacuum once the Ar was evacuated and the thermal treatment was carried out at 285°C for 72 h. The reducing treatment strategy is represented in Figure 1b.

Characterization techniques

The structural characterization was made by X-ray diffraction using a Philips PW 1820 apparatus equipped with a $\text{K}\alpha_1/\text{K}\alpha_2$ source and a copper anticathode. Diffraction patterns for V1, C1 and A1 samples were collected with a 2θ step of 0.02° between 10° and 60° for a measuring time of 10 h. The thermal treatment study of V1 sample was made by collecting X-ray

diffraction patterns from 20° to 60° 2θ with a counting time of 10 s per step. Patterns corresponding to V2, C2 and A2 samples were also collected employing these conditions.

Diffraction patterns of V1, C1 and A1 samples were refined employing the Fullprof program package, via Le Bail procedure (full pattern matching) using an isotropic Caglioti function for the peak profile fitting. From the peak width determined by the pattern refinement, the Debye Scherrer relation has allowed from various peaks dispersed on a wide range of 2θ angle getting the average crystallite diameter of the analyzed samples. The microstructural characterization was performed by Transmission Electron Microscopy with a LVMS microscope from DeLong instruments, working at 5 kV.

Luminescence spectra were collected using a FL212 SPEX (Jobin-Yvon) connected to a photomultiplier tube (R955 Hamamatsu PMT) detector. A Xenon lamp (450W) was used as the excitation source. Decay curves were collected on a Fluorolog 3 Horiba spectrofluorometer.

Results and discussion

Structural characterization

The unit cell of vaterite, calcite and aragonite crystalline structures obtained through the first synthesis route (Figure 1a) have been depicted in Figure 2 (a, b and c, respectively) together with an enlargement of each polyhedral site formed by the first coordination sphere of oxygen ligands around the M^{2+} cation. In the case of the hexagonal cell of vaterite,²² the cation is surrounded by six equidistant oxygen atoms describing an octahedron. In addition, two oxygen atoms at longer distance complete the overall 6+2 coordination geometry (Figure 2a). In the case of the hexagonal cell of the calcite (Figure 2b), the cation is enclosed by six oxygen atoms in a regular octahedron and in aragonite phase, the first coordination sphere is formed by nine oxygen atoms (Figure 2c).⁶

The X-ray diffraction patterns corresponding to the product obtained after each thermal treatment of V1 sample between room temperature and 700°C are collected in Figure 3. As it can be observed, for a temperature around 350°C the metastable vaterite phase obtained by the precipitation method evolves to calcite and if the treatment temperature is increased, the carbonate compound starts to decompose into the corresponding oxides (see patterns for 600 and 700°C).

The crystal structure of V1, C1 and A1 samples have been studied by full pattern matching refinement of their corresponding X-ray diffraction patterns using the $P6_3/mmc$, $R-3c$ or $Pmcn$ space groups, respectively.²³⁻²⁴ The experimental and calculated X-ray diffraction patterns together with the differential signals for as-prepared V1, C1 and A1 samples are represented in Figure 4. The indexed diffraction peaks can be ascribed to pure vaterite, calcite and aragonite phases (a, b and

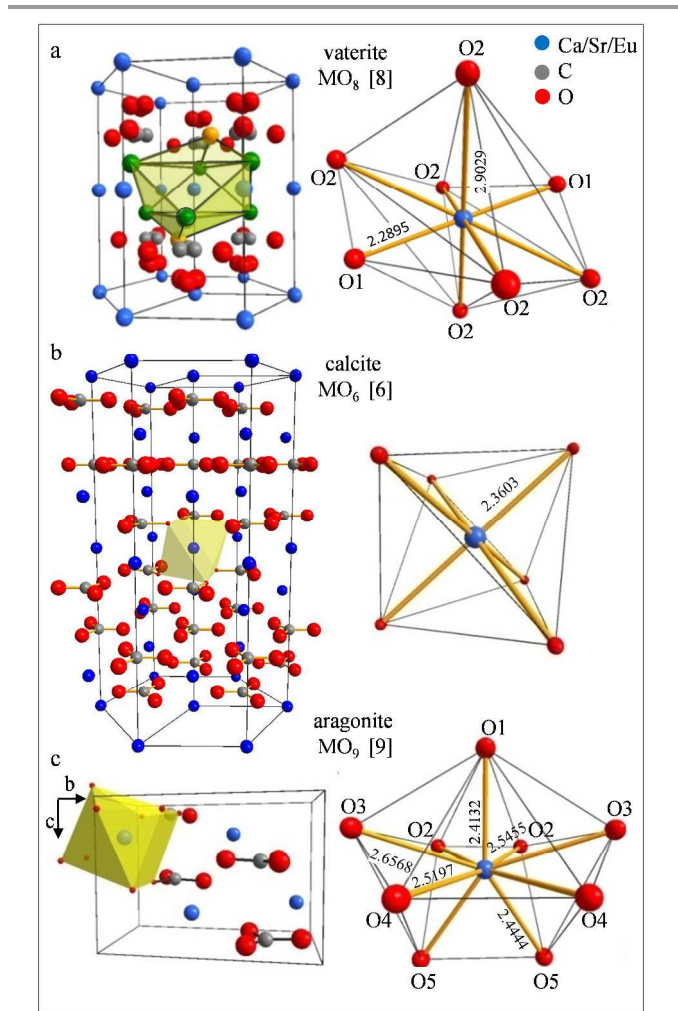


Figure 2. Structural cells corresponding to vaterite (a), calcite (b) and aragonite (c) allotropic forms. It has been represented the surrounding environment of the cation and the cation-oxygen distances are indicated as well. M: Ca, Sr

c respectively). However, in the case of A1 sample some traces of calcite were found after the mechanical treatment as it can be deduced by the reflection peak appearing at 29° 2θ that corresponds to the most intense peak of calcite.

The broad peaks observed in the case of V1 and A1 samples suggest they present lower crystal domain size than that corresponding to C1 sample. The cell parameters and the crystal domain dimensions obtained after the refinements, together with the reliability factors, are collected in Table 1 for each sample. The three structural phases exhibit slightly higher cell parameters than those found in the literature corresponding to pure CaCO_3 .²⁵⁻³⁰ This can be justified under the consideration of Sr^{2+} and in a less influential way Eu^{3+} , as both are larger than the host matrix Ca^{2+} cation.

Since only for SrCO_3 and CaCO_3 compositions, the aragonite structure can be stabilized at room temperature and ambient pressure, the cell parameters of the as-prepared aragonite Eu-doped $(\text{Ca,Sr})\text{CO}_3$ compound can be discussed basing on the cell parameters already reported for these two extreme compositions (SrCO_3 ,³¹⁻³³ and CaCO_3 ,²⁵⁻²⁷). Hence, considering

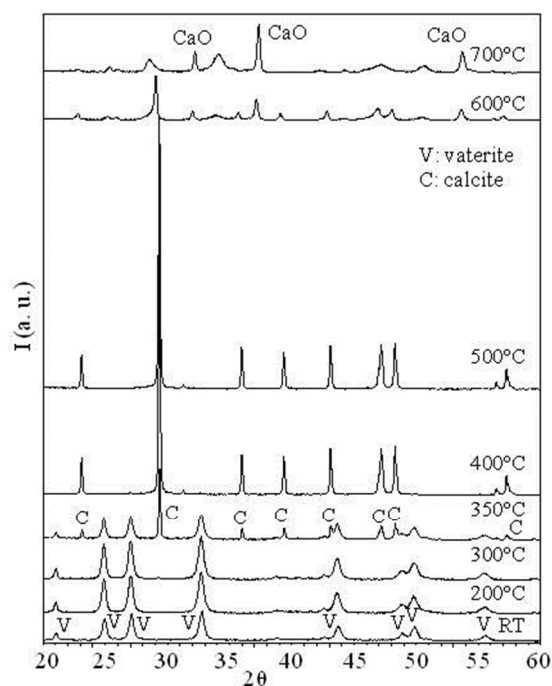


Figure 3. X-ray diffraction patterns corresponding to the phase evolution with temperature of V1 sample.

lattice parameters of $a = 4.95 \text{ \AA}$ and 5.09 \AA , $b = 7.97 \text{ \AA}$ and 8.40 \AA , $c = 5.74 \text{ \AA}$ and 6.02 \AA for CaCO_3 and SrCO_3 , respectively, the orthorhombic cell parameters of the as-prepared aragonite phase (Table 1) well satisfies the Vegard law by considering 20-25 mol % of strontium in substitution for calcium. The slight deviation between the experimental 30 mol % and the theoretical 20-25 mol % ratio, may be issued from a non-total precipitation of the strontium added in the initial solution. The accurate chemical composition, which is known to be difficult to evaluate by ICP analyses while calcium is in the composition, was not determined since it was preserved in the three allotropic forms and does not affect the discussion of the work.

TEM images showed in Figure 5 corresponding to V1 (Figure 5a-c), C1 (Figure 5d-e) and A1 (Figure 5f-h) carbonate samples show the microstructure associated with the synthesis process. In the case of V1 sample, the precipitation method leads to spherical aggregates with a diameter between 0.5 and 1.0 μm composed by particles with an average size of 20 nm (Figure 5b) which is in good agreement with our previous X-ray diffraction study (see Table 1). The spherical aggregates of 1.0 μm diameter corresponding to C1 sample, are clearly issued from the agglomerates of V1 sample, i. e. the polycrystalline particle morphology is preserved (Figure 5e). Obviously, the annealing step required to transform vaterite phase into calcite phase leads to a sintering of the particles justifying the large increase of the crystallite size observed from vaterite to calcite (Figure 5b, 5e). Also, the ball-milling treatment employed to obtain aragonite phase from vaterite, destroy the initial spherical aggregates observable in V1 sample and the aragonite

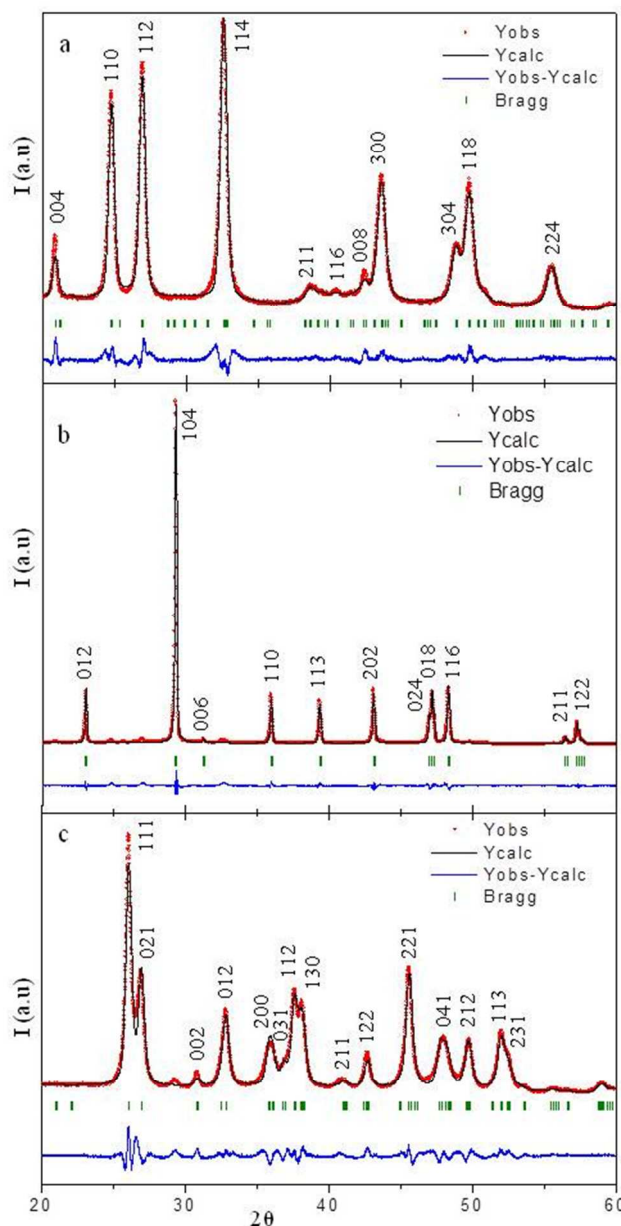


Figure 4. X-ray diffraction patterns of V1 (a), C1 (b) and A1 (c) samples. It has been depicted as well the calculated pattern obtained from profile refinement of the experimental one together with the difference between both, and the Bragg positions.

particles with a diameter around 15-20 nm are then easier to distinguish (Figure 5e-f). In addition, the pressure transferred by the shock of the agate balls during the mechanical treatment is enough to allow the phase transformation without breaking the crystals. The estimated particle size from TEM images is in good agreement with the crystal domain size obtained from full pattern matching refinement (see Table 1).

In Figure 6, the X-ray diffraction patterns belonging to the three samples obtained after the additional reducing treatment (V2, C2 and A2) are compared to those corresponding to raw compounds (V1, C1 and A1). The phases obtained can be ascribed to vaterite, calcite and aragonite crystal structures for

Table 1. Crystallographic data and crystal domain size corresponding to V1, C1 and A1 samples

Sample	Crystallographic data			Apparent size		Reliability factors	
	<i>a</i> (Å)	<i>b</i> (Å)	<i>c</i> (Å)	Max. (nm)	Min. (nm)	Rp	Rwp
V1	7.1889 (2)	7.1889 (2)	17.0479 (5)	21.6 ± 0.6	19.3 ± 0.6	4.32	5.87
C1	4.9986 (2)	4.9986 (2)	17.1974 (8)	208.0 ± 4.0	196.0 ± 4.0	8.28	11.3
A1	4.9772 (2)	8.0650 (3)	5.7985 (2)	16.3 ± 0.3	15.0 ± 0.3	12.7	12.7

V2, C2 and A2 samples, respectively. Hence, the low temperature reducing treatment allows preserving the three structural phases. The sharp diffraction maxima corresponding to the calcite structure (see maximum at 29° 2θ) exhibited by pattern of C2 sample in comparison with those corresponding to V2 and A2, reveals a larger particle size in this case accordingly with the larger size of the raw C1 sample. In addition, the three X-ray diffraction patterns show extra

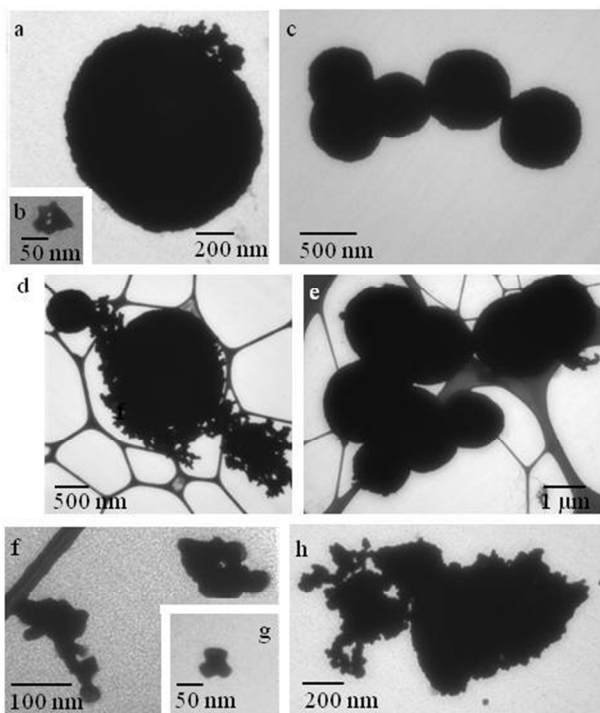


Figure 5. TEM images corresponding to V1 (a-c), C1 (d,e) and A1 (f-h) samples.

reflection maxima that can be indexed to CaO·H₂O (ICSD 64950) phase obtained as redox subproduct after oxidation of the calcium hydride. The diffraction peaks that can be ascribed to this white and non-luminescent phase are marked on the X-ray diffractograms. Taking into account the occurrence of this secondary phase in such a large quantity, the crystal size of V2,

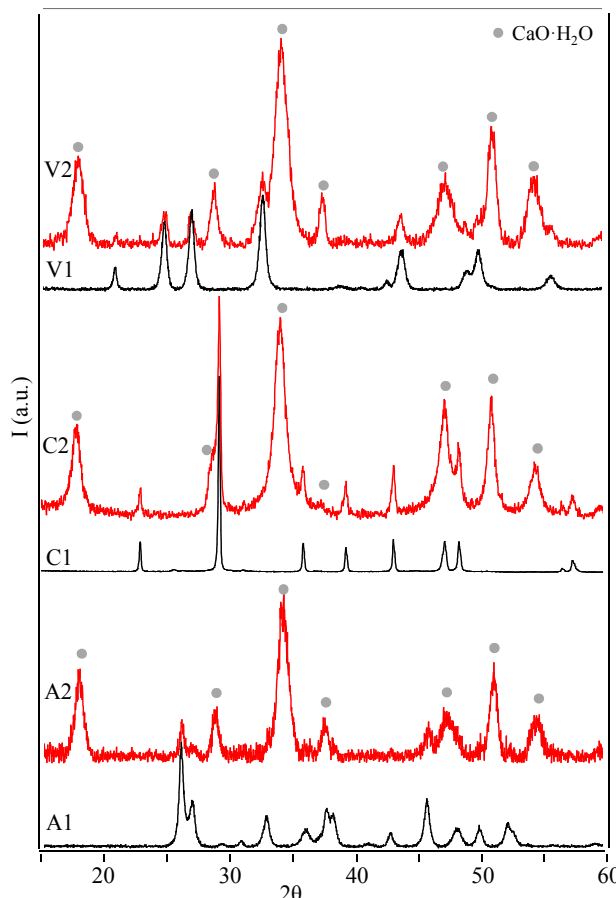


Figure 6. X-ray diffraction patterns for V2, C2 and A2 samples. Patterns corresponding to V1, C1 and A1 samples are also depicted as reference.

C2 and A2 samples was not analyzed by X-ray diffraction or TEM technique.

Photoluminescence properties

Results. In Figure 7 are depicted the excitation photoluminescence spectra (PLEx) and the emission photoluminescence spectra (PLEm) for V1, C1 and A1 samples. The PLEx spectra have been measured for the three samples in the wavelength range of 220-550 nm by monitoring with the intense red emission detected at 614 nm. The PLEm spectra for an excitation wavelength of 250 nm (and 270 nm in the case of A1 sample) which corresponds to the absorption energy of the O²⁻→Eu³⁺ charge transfer band (CTB), have been measured from 560 up to 750 nm. Sharp emission lines between 300 and 550 nm can be observed for the three structural host-lattices due to intra-configurational 4f-4f transitions of Eu³⁺.⁸⁻¹⁰ In the 560-720 nm range, the appearing emission lines common to the three samples have been identified as radiative transitions from the ⁵D₀ level of Eu³⁺ ions down to the fundamental manifold ⁷F_J. In the three cases, the maximal emission is due to the ⁵D₀→⁷F₂ electric dipole transition.

The fluorescence decay curve monitoring at 614 nm of ⁵D₀→⁷F₂ transition was measured for V1, C1 and A1 samples

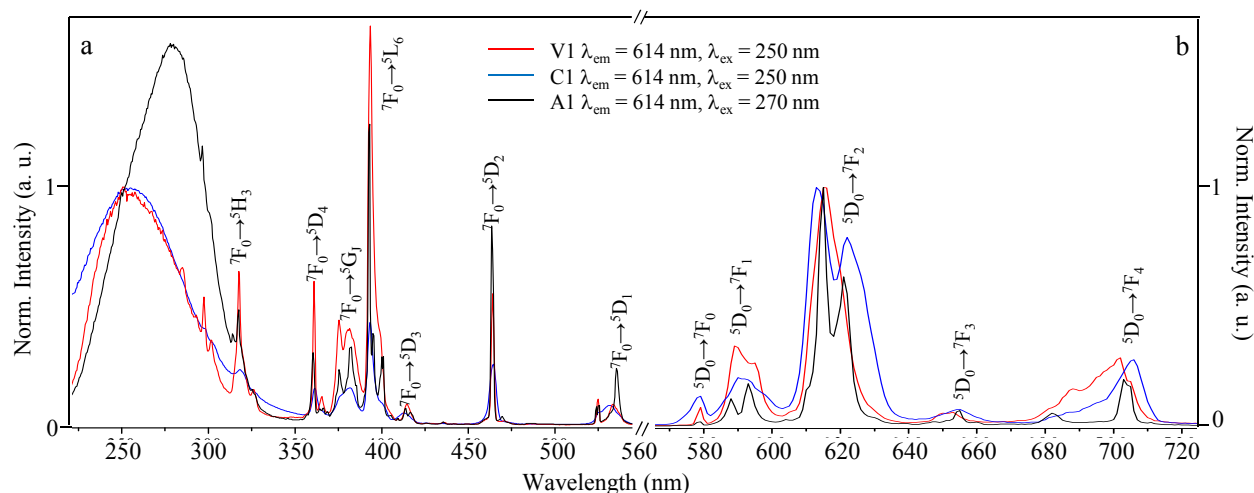


Figure 7. Normalized PLEx spectra at CTB (left) and normalized PLEm spectra at the maximum of emission (right), corresponding to V1, C1 and A1 samples. It is indicated the wave length emission and excitation for each sample.

under excitation at 250 nm in the charge transfer absorption band. The curves are depicted in Figure 8. The general expression of a decay curve can be expressed as follow:

$$I = \sum_{i=1}^n I_i \exp\left(-\frac{t}{\tau_i}\right), \quad (1)$$

with I_i : contribution intensity (can be expressed in contribution percentage for normalized initial intensity $I = 100$), τ_i : lifetime of the contribution i .

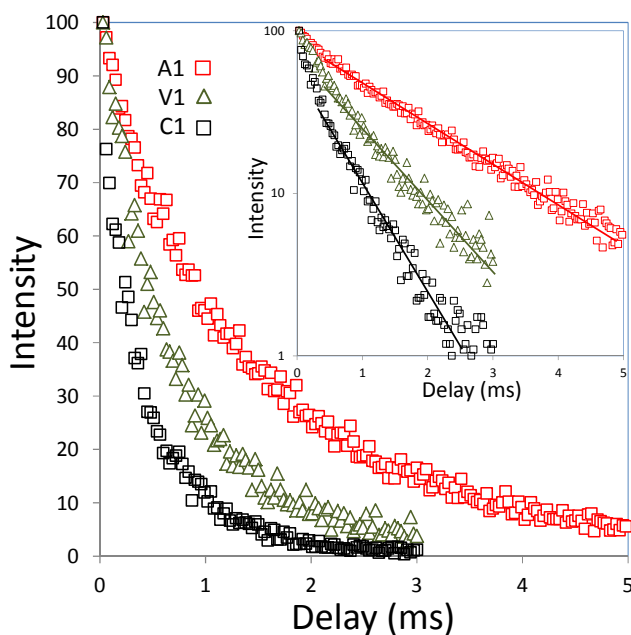


Figure 8. Fluorescence decay curves of ${}^5D_0 \rightarrow {}^7F_2$ transition of V1, C1 and A1 samples measured with an excitation wavelength of 250 nm.

For qualitative comparison, in both standard and semi-log scales, V1, C1 and A1 decay curves are superimposed in the Figure 8. It can be seen that the decay curves cannot correctly be fitted by a single exponential contribution. Indeed, in the

inset with semi-log scale, it can easily be seen that the decay curves are not strictly linear, which indicates a second contribution. We cannot discard an artificial increase of a non radiative contribution due to defect at the shortest times or trace of a second phase (calcite in the aragonite sample). Due to the relatively poor accuracy of the fluorescence decay experiments and taking into account that the aim of the study was to qualitatively compare the three samples, the choice was made in basis of not multiplying the contributions. Hence, none arbitrary fit is proposed. Whatever, the results show that the characteristic lifetimes are significantly increased from C1 to V1 and then A1 samples.

In Figure 9a it can be seen the raw PLEm spectrum of V1, C1 and A1 samples, recorded employing exactly same conditions. On the other hand, the photograph shown in Figure 9b illustrates the color and intensity emission of these samples under a 254 nm UV excitation.

It is shown in Figure 10 the PLEx spectra for V2, C2 and A2 samples measured in the wavelength range of 220-550 nm by monitoring with the emission detected at 530, 500 and 540 nm depending on the structure. The observable shoulders in the PLEx spectra correspond to the splitting of all the 5d orbitals. The PLEm spectra from 560 up to 750 nm are also depicted for the three samples for an excitation wavelength of 320 nm (and 464 nm in the case of A2 sample).

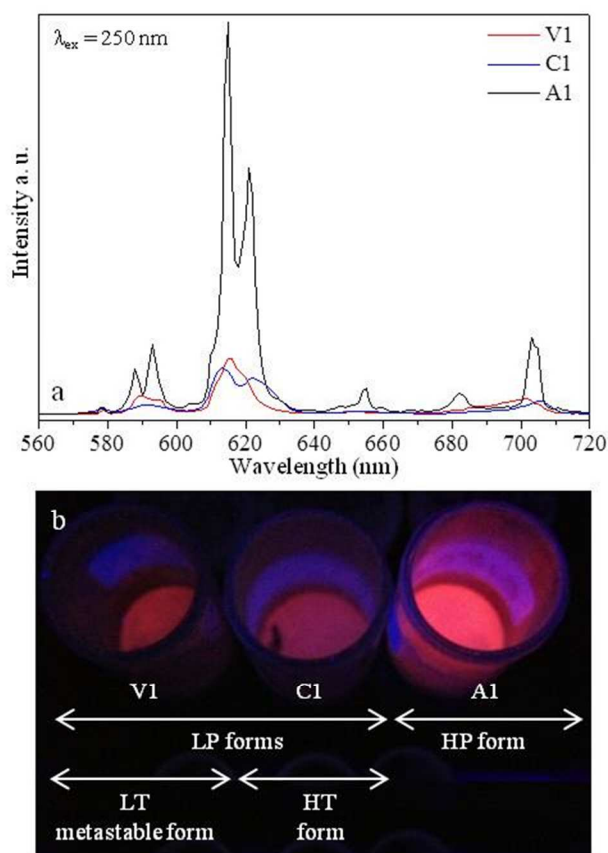


Figure 9. Raw PLEm spectra for V1, C1 and A1 samples (a). In (b) it is shown an image of the three samples after being irradiated at 254 nm. LP, HP, LT and HT refer to low-pressure, high-pressure, “low-temperature” and high-temperature forms, respectively.

Discussion. The photoluminescence studies confirm the location of the doping element in different environment depending on the allotropic form of the stabilized carbonate.

While V1 and C1 samples exhibit a CTB located at 250 nm, in the case of A1 sample, the CTB is shifted to lower energy (Figure 7a) due to the low covalence Eu-O bond associated with the higher coordination number characteristic of the aragonite phase (see Figure 2c). When the coordination number increases and considering that the environment of all oxygen atoms is equivalent, the average bond length increases concomitantly with the decrease of both the covalence and the bond strength.³⁴ This red shift effect of oxygen to cation CTB versus an increase of the cation coordination number associated to a change of the crystalline allotropic form is, for instance, at the origin of the thermochromic/piezochromic phenomena of the AMoO_4 compounds.³⁴⁻³⁶

On the other hand, the occurrence of the $^5\text{D}_0 \rightarrow ^7\text{F}_2$ electric dipole transition in the PLEm spectra for V1, C1 and A1 samples, evidences the non-centrosymmetric environment of the europium element whatever the host-lattice. The lack of inversion center in a crystallographic site favors the mixing between the 4f even orbitals and 5d odd orbitals leading to an increase of the electric dipole transition probability with an emission located in the red part of the electromagnetic range.³⁷

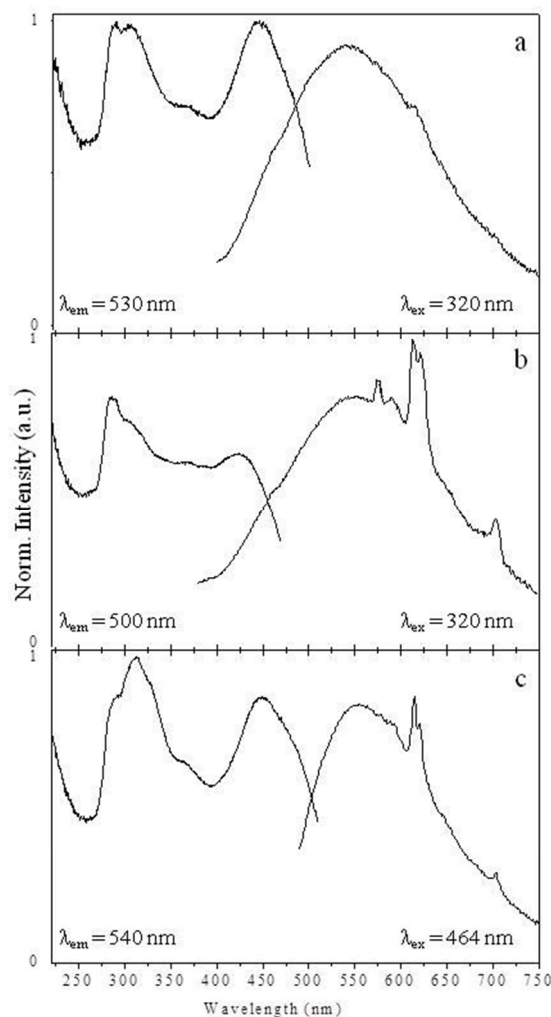


Figure 10. PLEx (left) and PLEm (right) spectra corresponding to V2 (a), C2 (b) and A2 (c) samples.

In this sense, the site asymmetry can be evaluated for each structure from the ratio of the areas of the normalized peaks between the red $^5\text{D}_0 \rightarrow ^7\text{F}_2$ electric dipole transition and the orange $^5\text{D}_0 \rightarrow ^7\text{F}_1$ magnetic dipole transition as indicated in eq. (2).³⁸

$$R/O = \frac{{}^5\text{D}_0 \rightarrow {}^7\text{F}_2}{{}^5\text{D}_0 \rightarrow {}^7\text{F}_1} \quad (2)$$

The obtained red/orange ratios (R/O ratios) are calculated to be equal to 3.2, 5.9 and 6.4 for respectively V1, C1 and A1 samples. The R/O ratios are known to increase for more distorted local coordination spheres.^{38,39} Thus, these ratios indicate that aragonite and calcite phases are the ones presenting the most asymmetric europium coordination sphere leading to a deeper red emission. While this phenomenon is expected for A1 sample in which the alkaline earth site of the host matrix is already described by five different cation-oxygen distances (Figure 2c), it is surprising however for C1 sample in which the expected coordination sphere is a regular octahedron (Figure 2b). It is observed that C1 sample presents a larger and not so-well defined profile spectrum like the other two samples.

This fact reflects a strong perturbation of the lattice when incorporating the doping element, probably due to the low coordination number and low cation-oxygen distance offered by the matrix. Therefore, the high lattice perturbation around the phosphor dopant would be responsible for the crystal-site asymmetry associated to a deep red emission in the case of C1 sample. In addition, as europium is stabilized at the 3+ oxidation state, local punctual defects have to compensate this excess of positive charge. One can imagine an oxygen vacancy is created for one trivalent europium couple of species, giving rise to a perturbed local environment. This kind of consideration should obviously create perturbations in a more intense way inside the allotropic form offering the lowest coordination numbers as in calcite.

On the other hand, the so low emission intensity exhibited by V1 and C1 samples in comparison with that of A1 sample (Figure 9a) could be justified under several considerations. For V1 and C1 samples, the intensity ratio between the CTB and the 4f line, is small. This can be explained by an internal configurational quenching due to a direct non radiative transfer from the CTB down to the fundamental 7F_3 manifold. The spectral distribution intensity between the CTB and the 4f is also strongly affected by the size of the luminescent particles. A nanometric size distribution can artificially enhance the 4f-4f transition in absorption due to successive absorption-reflection-transmission process through the whole particle. This can clearly contribute to a better excitation efficiency of the A1 sample. Also, many authors,²⁴ point out that structural vacancies associated to the charges compensation $\square + 2Eu^{3+} \rightarrow 3M^{2+}$ may decrease the luminescence response due to the high effectiveness of the energy transfer between $Eu^{3+} \rightarrow \square$ that would not participate in the radiative de-excitation decay process. However, in the case of the prepared samples the luminescence property may not be drastically affected by this process as this effect seems to be important for concentration of Eu higher than 15%.²⁴ Furthermore, it is not neither expected a concentration-quenching effect associated to high concentrations of Eu with an energy loss in a non-radiation process between proximal Eu atoms. In addition, a small shoulder can be visualized around 610 nm in the raw PLEm spectrum of A1 sample (Figure 9a), that may correspond to remaining traces of calcite as discussed before.

The metastable “low-temperature” phase (vaterite) and the high-temperature phase (calcite) could be experimentally differentiated by considering their spectral distribution and red/orange ratio. Therefore, by measuring this feature in PLEm spectra, raw vaterite material could be employed as thermal sensor to know if an increment of temperature has occurred in the 350-500°C range. Also, the different luminescence properties observed between the high-pressure (aragonite) and low-pressure (vaterite, calcite) forms, leads to believe raw vaterite (or calcite) material as useful shock detector by employing a 254 nm commercial UV light to radiate the carbonate material.

The fitting of the decay curve also puts in evidence that several contributions (at least two contributions) have to be taken into account in the global radiative de-excitation process. The decay time calculated for A1 sample is close to those observed for standard phosphors as Eu-doped Y_2O_3 or Eu-doped $GdBO_3$ ^{40,41} and the faster decay times of V1 and C1 samples may be related with the PL killer centers (local defects, concentration) found in these materials.

Concerning V2, C2 and A2 samples, they can be excited in the UV and present broad emission bands centered in the green region accordingly with the reduction of the europium ion at the +2 oxidation state.¹⁹ The emission band presents a maximum at 530 nm regardless the host matrix indicating that Eu^{2+} luminescence does not fully succeed into discriminating the three allotropic forms. In addition to the large bands, sharp emission lines are observed around 620 and 700 nm which indicate the redox reaction has not been completely achieved and like in other studies collected in the literature, there are traces of Eu^{3+} ions.^{42,43} The reduction process leads to reduction of part of the europium at the divalent oxidation state. But the relative intensity between the expected allowed 5d-4f Eu(II) transition and the forbidden 4f-4f Eu(III) transitions indicates that the efficiency of Eu(II) is really low. Taking into account the larger atomic volume in the case of Eu^{2+} (1.20 Å) in comparison with Eu^{3+} (0.99 Å), it could be said that in the case of vaterite structure which presents the largest cation-anion distances, the Eu^{3+} would be more easily reduced in accordance to a larger crystal site where Eu^{2+} would be placed. On the contrary, calcite structure would difficult the Eu^{3+} reduction due to shorter Eu-O distances.

Conclusions

Pure (Ca,Sr)CO₃:Eu³⁺ vaterite was obtained by the precipitation method. This metastable phase transforms with the temperature (at about 350°C) into calcite phase and into the aragonite high-pressure phase when an additional ball-milling step is applied. These three different allotropic forms can be easily obtained thanks to the incorporation of 30 mol% of strontium in place of calcium. The structure of the three allotropic forms was studied by profile refinement of the corresponding X-ray diffraction patterns. Cell parameters are coherent with literature data on the extreme compositions CaCO₃ and SrCO₃ considering a Vegard law.

From the Eu(III)-doped forms, it was possible to obtain the corresponding forms with divalent oxidation state for europium ions thanks to the employment of CaH₂. The three obtained Eu(II)-doped compounds emit in the same range of wavelength and therefore it was not possible to distinguish the three samples by luminescence. Furthermore, the reduction is difficult to fully achieve and traces of Eu^{3+} can be detected. However, luminescent measurements on the Eu(III)-doped materials allow differentiating not only between the « low-temperature » metastable vaterite and high-temperature calcite phase, but also between the low-pressure forms (vaterite and

calcite) and the high-pressure one (aragonite). In this sense it has been found different red/orange emission intensities ratio and different profile PL spectra. The different luminescent properties found for each carbonate structure, offer the possibility to employ this system as indicator for a temperature variation from 350 up to 500°C and also for shocks.

Acknowledgements

This project has received funding from the European Union's Seventh Framework Programme for research, technological development and demonstration under grant agreement no 284562.

Notes and references

[†]CNRS, ICMCB, UPR 9048, F-33600 Pessac, France

[‡]Univ. Bordeaux, ICMCB, UPR 9048, F-33600 Pessac, France

- R. M. Santos, P. Ceulemans and T. Van Gerven, *Chem. Eng. Res. Des.*, 2012, **90**, 715.
- M. Fernandes Marques, T. Stumpf, T. Rabung, D. Bosbach and Th. Fanghänel, *Geochim. Cosmochim. Acta.* 2008, **72**, 464.
- F. Heberling, M.A. Denecke and D. Bosbach, *Environ. Sci. Technol.* 2008, **42**, 471.
- M. Schmidt, T. Stumpf, C. Walther, H. Geckeis and T. Fanghänel, *J. Colloid Interf. Sci.*, 2010, **351**, 50.
- W. D. Carlson, *American Mineralogist.*, 1980, **65**, 1252.
- A. R. Oganov, C. W. Glass and S. Ono, *Earth Planet. Sci. Lett.*, 2006, **241**, 95.
- Y. Pan, M. Wu and Q. Su, *Mat. Res. Bull.* 2003, **38**, 1537.
- V. Juberá, J. Chaminade, A. Garcia, F. Guillen and C. Fouassier, *J. Lumin.* 2003, **101**, 1.
- M. Yang, Q. Huang and X. Jin, *Colloid. Surf. A: Physicochem. Eng. Asp.* 2011, **386**, 87.
- Y. Li, J. Zhang, X. Zhang, Y. Luo, S. Lu, X. Ren, X. Wang, L. Sun and C. Yan, *Chem. Mater.* 2009, **21**, 468.
- R. D. Shannon, *Acta Cryst.*, 1976, **A32**, 751.
- M. Kang, J. Liu, G. Yin and R. Sun, *Rare Met.* 2009, **28**, 439.
- M. Schmidt, T. Stumpf, C. Walther and H. Geckeis, *Dalton Trans.* 2009, 6645.
- L. Z. Lakshtanov and S. L. Stipp, *Geochim. Cosmochim. Acta.* 2004, **68**, 819.
- B. Zhou, B. Liu B., H. Zou, Y. Song, L. Gong, Q. Huo, X. Xu, Y. Sheng, *Colloid. Surf. A: Physicochem. Eng. Asp.* 2014, **447**, 166.
- S.P. Bao, X.Y. Chen, Z. Li, B.J. Yang, Y.C. Wu, *Cryst. Eng. Comm.* 2011, **13**, 2511.
- Z. Ci, Y. Wang, *J. Electrochem. Soc.* 2009, 156, J267.
- J. Garcia-Guinea, E. Crespo-Feo, V. Correcher, A. Cremades, J. Rubio, L. Tormo, P.D. Townsend, *Radiat. Meas.*, 2009, **44**, 338.
- H. Xia, J. Zhang, J. Wang, Q. Nie and H. Song, *Mater. Lett.*, 2002, **53**, 277.
- P. Rack and P. Holloway, *Mater. Sci. Eng.*, 1998, **R21**, 171.
- M. Tukiá, J. Hölsä, M. Lastusaari and J. Niitykoski, *Opt. Mater.*, 2005, **27**, 1516.
- L. Kabalah-Amitai, B. Mayzel, Y. Kauffmann, A. N. Fitch, L. Bloch, P. U. P. A. Gilbert and B. Pokroy, *Science*, 2013, **340**, 454.
- D. A. Kulik, V. L. Vinograd, N. Paulsen and B. Winkler, *Phys. Chem. Earth.*, 2010, **35**, 217.
- J. Nara and S. Adachi, *J. Appl. Phys.*, 2013, **113**, 033519.
- E. N. Caspi, B. Pokroy, P. L. Lee, J. P. Quintana and E. Zolotoyabko, *Acta Cryst.*, 2005, **B61**, 129.
- A. del Negro and L. Ungaretti, *Am. Mineralog.*, 1971, **56**, 768.
- T. Pilati, F. Demartin and C. M. Gramaccioli, *Acta Cryst.*, 1998, **B54**, 515.
- S. M. Antao and I. Hassan, *Can. Mineralog.*, 2010, **48**, 1225.
- B. Pokroy, J. S. Fieramosca, R. B. von Dreele, A. N. Fitch, E. N. Caspi and E. Zolotoyabko, *Chem. Mater.*, 2007, **19**, 3244.
- E. Mugnaioli, I. Andrusenko, T. Schueler, N. Loges, R. E. Dinnebier, M. Panthofer, W. Tremel and U. Kolb, *Angew. Chem. Int. Ed.*, 2012, **51**, 7041.
- D. Jarosch and G. Heger, *Bull. Mineralog.*, 1988, **111**, 139.
- S. M. Antao and I. Hassan, *Can. Mineralog.*, 2009, **47**, 1245.
- I. D. Brown and D. Altermatt, *Acta Cryst.*, 1985, **B41**, 244.
- L. C. Robertson, M. Gaudon, S. Jobic, P. Deniard and A. Demourgues, *Inorg. Chem.*, 2011, **50**, 2878.
- M. Gaudon, A. E. Thiry, A. Largeteau, P. Deniard, S. Jobic, J. Majimel and A. Demourgues, *Inorg. Chem.*, 2008, **47**, 2404.
- M. Gaudon, C. Carbonera, A. E. Thiry, A. Demourgues, P. Deniard, C. Payen, J. F. Létard and S. Jobic, *Inorg. Chem.*, 2007, **46**, 10200.
- G. Blasse and B. Grabmaier, *Luminescent Materials*, Springer, Berlin Heidelberg, New York, 1994
- Y. Wu, Y. Nien, Y. Wang and I. Chen, *J. Am. Ceram. Soc.*, 2012, **95**, 1360.
- R. Reisfeld, E. Zigansky, M. Gaft, *Molecular Phys.*, 2004, **102**, 1319.
- A. Bril and W. L. Wanmaker, *J. electrochem. Soc.*, 1964, **111**, 1363.
- G. Blasse, *J. Chem. Phys.*, 1966, **45**, 2356.
- V. B. Pawade and S. J. Dhoble, *J. Lum.*, 2013, **135**, 318.
- L. Wondraczek, S. Krolkowski, P. Nass, *J. Mater. Chem. C*, 2013, **1**, 4078.